Theor Chem Acc (2002) 107:154–161
DOI 10.1007/s00214-001-0312-z

Theoretical
Chemistry Accounts

Regular article

A theoretical study of photoinduced electron transfer between tetracyanoethylene and arene

Li Xiang-Yuan, Yi Hai-Bo, Li Ze-Rong, He Fu-Cheng

College of Chemical Engineering, Sichuan University, Chengdu 610065, China

Received: 30 April 2001 / Accepted: 18 October 2001 / Published online: 9 January 2002

Abstract. Ab initio calculations have been performed to investigate the state transition in photoinduced electron transfer reactions between tetracyanoethylene and biphenyl as well as naphthalene. Face-to-face conformations of electron donor–acceptor (EDA) complexes were selected for this purpose. The geometries of the EDA complexes were determined by using the isolated optimized geometries of the donor and the acceptor to search for the maximum stabilization energy along the center-to-center distance. The correction of interaction energies for basis set superposition error was considered by using counterpoise methods. The ground and excited states of the EDA complexes were optimized with complete-active-space self-consistent-field calculations. The theoretical study of the ground state and excited states of the EDA complex in this work reveals that the S_1 and S_2 states of the EDA complexes are charge–transfer (CT) excited states, and CT absorption which corresponds to the $S_0 \rightarrow S_1$ and $S_0 \rightarrow S_2$ transitions arise from $\pi-\pi^*$ excitation. On the basis of an Onsager model, CT absorption in dichloromethane was investigated by considering the solvent reorganization energy. Detailed discussions on the excited state and on the CT absorptions were made.

Key words: Photoinduced electron transfer – Charge separation – Excited state – Solvation energy

1 Introduction

The investigation of intermolecular photoinduced electron transfer (PET) of organic compounds is of considerable importance both in theory and in experiment. PET reactions between tetracyanoethylene (Tcne) and a series of arenes as well as olefins have attracted much attention recently. A number of experiments showed that a new absorption in visible region could be observed when arene and Tcne are mixed [1, 2, 3, 4]. These wavelengths of absorption are explicitly longer than those of Tcne (260 [5] or 270 nm [6]) and those of arene species, for example, 246 nm for biphenyl (Bip) [7]. It is widely believed that the new absorption arises from the excitation of an electron donor–acceptor (EDA) complex and results in the formation of a charge-transfer (CT) state.

The mechanism of PET reactions has been studied in various experiments and theoretical calculations; however, more direct theoretical evidence of photoinduced charge separation and theoretical studies on the solvent effects on PET reactions will lead to better understanding of microscopic aspects of PET processes. As a kind of photochemistry reaction, the mechanism of the photoexcitation and the back ET may be schematically described by the following simplified form:

$$\underset{\text{precursor}}{D + A \rightarrow [D\cdots A]_p} \overset{h\nu}{\rightarrow} \underset{\text{precursor}}{{}^1[D^+\cdots A^-]_p} \rightarrow$$

$$\underset{\text{successor}}{{}^{1,3}[D^+\cdots A^-]_s} \rightarrow \underset{\text{successor}}{[D\cdots A]_s} \rightarrow \underset{\text{precursor}}{[D\cdots A]_p}$$

We use here subscript 'p' to refer to the precursor geometry, i.e., the equilibrium geometry of the EDA complex, and 's' to successor geometry, i.e., the equilibrium geometry of ion pair. The mechanism encompasses the following processes: the formation of the EDA complex $[D\cdots A]_p$ (or precursor complex), the formation of the CT excited state ${}^1[D^+\cdots A^-]_p$ by the photoexcitation of the EDA complex with the geometry unchanged (Franck–Condon principle), the relaxation of the CT excited state ${}^1[D^+\cdots A^-]_p$ from the equilibrium geometry of the precursor to the geometry of the ion pair (${}^{1,3}[D^+\cdots A^-]_s$, successor geometry), the charge recombination (CR) of the successor, and the motion from the CR complex ($[D\cdots A]_s$, the successor geometry) to the precursor complex $[D\cdots A]_p$ along the potential-energy surface of the ground state. In addition, intersystem crossing may occur in the process of the relaxation of the CT excited state, i.e. ${}^1[D^+\cdots A^-]_p \rightarrow {}^3[D^+\cdots A^-]_s$. In the

Correspondence to: Li Xiang-Yuan
e-mail: xyli@scu.edu.cn

CR process, the back ET is possibly accompanied by CT emission.

We investigated the PET reactions between Tcne and Bip or naphthalene (Nap) by optimizing the ground state and the CT excited states of EDA complexes as well as equilibrium ion pairs. The mechanisms are supposed as follows:

$$[\text{Tcne}\cdots\text{Bip}]_p \xrightarrow{h\nu} {}^1[\text{Tcne}^-\cdots\text{Bip}^+]_p \rightarrow {}^{1,3}[\text{Tcne}^-\cdots\text{Bip}^+]_s \rightarrow [\text{Tcne}\cdots\text{Bip}]_s \quad (1)$$

$$[\text{Tcne}\cdots\text{Nap}]_p \xrightarrow{h\nu} {}^1[\text{Tcne}^-\cdots\text{Nap}^+]_p \rightarrow {}^{1,3}[\text{Tcne}^-\cdots\text{Nap}^+]_s \rightarrow [\text{Tcne}\cdots\text{Nap}]_s \quad (2)$$

2 Geometries of donor and acceptor

2.1 Bip and Nap

Neutral Bip is an interesting molecule because of the existence of a torsional angle between the two phenyl rings observed in experiments [8]. Our previous calculations revealed that there is a torsional angle of about 45° around the interring C_1-C_2 [9], and the geometry optimization at the level of unrestricted Harbree–Fock (UHF) 6-31G** indicates that Bip has D_2 symmetry with the principle axis being perpendicular to the interring C_1-C_2 bond. The torsional angle of 42.80° obtained is close to the experimental value [8,10]. Good agreement with experimental results was achieved by some authors from theoretical calculation of the biphenyl torsion angle [9, 11, 12]. Their calculation gave a torsion potential barrier of 12–20 kJ mol^{-1}. On the other hand, the geometry optimization indicates that all the carbon atoms in the biphenyl cation (Bip^+) lie on the same plane, so D_{2h} symmetry was used for the optimization of Bip^+. Both neutral Nap and its cation radical (Nap^+) were optimized with the constraint of D_{2h} symmetry. The planar structures of both the neutral Nap molecule and its cation radical were optimized at the level of UHF/6-31GG**.

The ionization potential (IP) of the donor in the PET reaction is a crucial quantity for the electronic spectra. Empirical relationships between the IP of the donor and the CT absorption were suggested for Tcne-donor systems [1, 3, 13]. The transition energy (E_{CT}), which corresponds to the CT process, is related to the IP of the donor with a certain acceptor by the expression [3]

$$E_{CT} = hc/\lambda_{max} = IP_D - EA + \text{constant}\ , \quad (3)$$

where λ_{max} is the wavelength of maximum absorbance of the CT band, which corresponds to the vertical $S_0 \rightarrow S_1$ transition, IP_D is the IP of the donor, and EA is the electronic affinity of Tcne.

The HF self-consistent-field (SCF) calculations of the IP based on Koopmans' theorem sometimes lose quantitative accuracy; therefore, we calculated the vertical IP of Bip and Nap by using the complete-active space SCF (CASSCF) method with 6-31G** basis sets. The CASSCF wave function is constructed by distributing eight active electrons in eight active π orbitals, denoted as CASSCF(8,8). For the corresponding cations, the CASSCF wave function is constructed by distributing seven active electrons in eight active orbitals, denoted as CASSCF(8,7). By using the equilibrium geometry of the donor, the gas-phase energies were calculated and the results are listed in Table 1. These results are acceptable compared with the experimental values. As shown in Table 1, the ionization potential of Bip is lower than that of Nap by 0.41 eV from our calculation. According to the relationship shown in Eq. (3), it may be predicted that [Tcne···Bip] should yield a longer wavelength of CT absorption from both the experimental IP values and the theoretically calculated ones.

2.2 Tetracyanoethylene

Tcne is a ubiquitous organic oxidant, and it becomes a strong electron acceptor in ET reactions. The wavelength of the maximum electronic absorbance, corresponding to the $S_0 \rightarrow S_1$ transition of Tcne molecule, was found to be 260 nm [5] or 270 nm [6]. In the present work, the neutral Tcne and its anion radical ($Tcne^-$) were optimized with the constraint of D_{2h} symmetry at the level of UHF/6-31G**. The labels of the atoms are shown in Fig. 1. The planar structures of both the neutral molecule and the anion radical were obtained. We found that the total energy of the equilibrium $Tcne^-$ is lower than that of the equilibrium Tcne by 2.73 eV from UHF/6-31G** calculations. The optimized bond lengths and the X-ray experimental values [6] of Tcne are given in Fig. 1. The bond lengths indicate that C_1-C_2 is a typical double bond and that C_4-N_8 is a typical triple bond, but that C_2-C_4 mediates between a single bond and a double bond.

Table 1. Ionization potentials (*IP*) of biphenyl (*Bip*) and naphthalene (*Nap*)

	$E_t(D)$[a]	$E_t(D^+)$[a]	IP_D[b]
Bip	−460.27621	−460.00035	7.50 (7.95)
Nap	−383.42738	−383.13673	7.91 (8.14)

[a] Total energies of neutral D and cation D^+ (au)
[b] Vertical IP in the gas-phase (eV). The experimental values [17] are given in *parentheses*

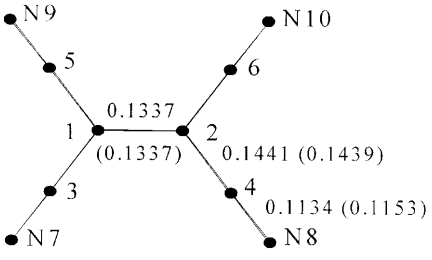

Fig. 1. The structure of planar Tene. The bond parameters of Tene are given in nanometers, and the experimental values are given in *parentheses*

Although the energy difference between the equilibrium Tcne$^-$ and equilibrium Tcne is calculated to be 2.73 eV, we may not expect to acquire a good EA value by a simple HF calculation. In pursuing a more accurate EA, we performed the CASSCF calculations, considering the electron correction. We calculated the total energy of the equilibrium Tcne at the level of CASSCF(8,8)/6-31G**, and that of the equilibrium Tcne$^-$ at the level of CASSCF (8,9)/6-31G**. The treatment for Tcne$^-$ means that we use the same active space but distribute nine active electrons in it. Thus we acquired the total energies for Tcne and Tcne$^-$ as follows: $E_t(\text{Tcne}) = -444.97210$ au, $E_t(\text{Tcne}^-) = -445.02116$ au.

From the total energies, one can see that the value of the EA of Tcne, 1.34 eV, has be improved when compared with the value of 1.6 eV given by other authors from experimental observation [11, 15, 16].

3 EDA complex and ion pair

3.1 Geometry of EDA complex

The formation of stable EDA complexes can be attributed to molecular interaction. The structures of such complexes may take two fashions, i.e, coplanar and face-to-face. Both X-ray experiment and theoretical calculations [3, 17, 18, 19, 20] revealed that the latter fashion of the EDA complex is more stable, because such an arrangement allows the maximum overlap between the π-type molecular orbitals in the two moieties [4, 18]. So we selected the face-to-face fashion in our theoretical study, in which the central C=C bond of Bip is parallel to the C=C bond of Tcne. Similarly, the central bridge C=C bond of Nap is placed parallel to the C=C bond of Tcne. The geometry of $[\text{Tcne}\cdots\text{Bip}]_p$ has C_2 symmetry owing to the torsion of 42.80° in Bip, while there is C_{2v} symmetry for the face-to-face complex of $[\text{Tcne}\cdots\text{Nap}]_p$. Instead of full geometry optimization, the geometries of the EDA complexes were determined by searching for the minimum of the total energy against the center-to-center distance, maintaining isolated optimized geometries of the donor and acceptor fixed. The stabilization energy (E_s) of the [D···A] complex is defined as

$$E_s = E(\text{D}) + E(\text{A}) - E(\text{D}\cdots\text{A}) \ , \qquad (4)$$

where E represents the equilibrium energy of the corresponding species. In this way, E_s is obtained as 12.36 kJ mol^{-1} for $[\text{Tcne}\cdots\text{Bip}]_p$ and 13.09 kJ mol^{-1} for $[\text{Tcne}\cdots\text{Nap}]_p$. Since the molecular interaction in the supermolecule is very weak, it is necessary to consider the effects of the basis set superposition error (BSSE) in calculating the stabilization energy of the [D···A] complex. In our calculation, the counterpoise method of Boys and Bernardi [24] was applied to consider the effect of BSSE [22, 23, 24]. The center-to-center distance is determined on the basis of the counterpoise-corrected potential-energy surface, and the "ghost" technique was used to extend the basis sets of the isolated donor and acceptor species. The counterpoise-corrected stabilization energy (E_s^{cp}) can be written as

$$E_s^{cp} = E^{DA}(\text{D}) + E^{DA}(\text{A}) - E(\text{D}\cdots\text{A}) \ , \qquad (5)$$

where E_s^{cp} is the stabilization energy corrected by the counterpoise method, and $E(\text{D}\cdots\text{A})$ is the total energy of the [D···A] complex as appears in Eq. (4), $E^{DA}(\text{D})$ and $E^{DA}(\text{A})$ are, respectively, the donor and acceptor energies calculated by using the expanded basis sets. The potential–energy calculations were performed at the level of HF/6-31G, and the stabilization energy of the EDA complex reaches its maximum value of 9.86 kJ mol^{-1} for $[\text{Tcne}\cdots\text{Bip}]_p$ at $d = 0.44$ nm and 8.58 kJ mol^{-1} for $[\text{Tcne}\cdots\text{Nap}]_p$ at $d = 0.42$ nm (Fig. 2). Nevertheless, in the case of no BSSE correction, we found that $[\text{Tcne}\cdots\text{Bip}]_p$ reaches the maximum stabilization energy at $d = 0.41$ nm, and $[\text{Tcne}\cdots\text{Nap}]_p$ reaches the maximum at $d = 0.40$ nm. This indicates that the BSSE influences not only the stabilization energy, but also the equilibrium geometry of the complex.

3.2 Groundstate and CT excited state

After the determination of the equilibrium donor–acceptor distance, the electronic ground state, S_0, of the EDA complex was optimized using the CASSCF method and 6-31G basis sets. We chose six active orbitals and distributed six electrons in these π-type active orbitals, thus denoted as CASSCF(6,6). According to the Franck–Condon principle, the geometry will remain unchanged during the photoexcitation of the EDA complex. In this work, the lowest singlet excited state, S_1, and the next lowest singlet excited state, S_2, of the EDA complex were calculated at the same level as the ground state. The state symmetry, the main configuration that contributes the largest component to the state, and the state energies are collected in Table 2.

From the Mulliken population analyses of the CASSCF wave functions, the net charges of the atoms in the EDA complexes are given in Fig. 3a and c. By suming the net charges over the atoms of the donor and the acceptor, we can find that both of the moieties are almost neutral in the ground state, so as to produce a negligibly small dipole moment in the direction from Tcne to the donor (Table 2).

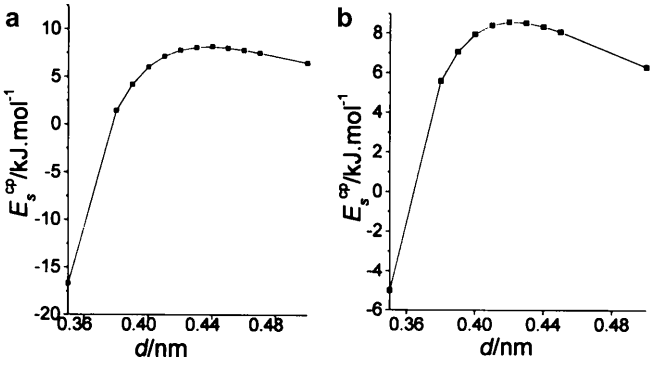

Fig. 2. Plots of the stabilization energy, E_s^{cp}, of **a** $[\text{Tcne}\cdots\text{Bip}]_p$ and **b** $[\text{Tcne}\cdots\text{Nap}]_p$ against the distance, d, between the two centers of the donor and the acceptor

Table 2. Energies of the ground state and low-lying excited states of electron donor–acceptor complexes using CASSCF(6,6)/6-31G calculations at their equilibrium geometries. *RE* is the relative energy with the energy of the ground state, −904.80931 au for $[Tcne\cdots Bip]_p$ and −827.95685 au for $[Tcne\cdots Nap]_p$, being taken as zero

	State	Symmetry	Main configuration[a]	RE/eV	D/D[b]
$[Tcne\cdots Bip]_p$ (C_2)	S_0	^1A	$38a^2 34b^2 35b^2 36b^0 39a^0 40a^0$ (0.967)	0.0	~0
	T_1	^1A	$38a^2 34b^2 35b^1 36b^1 39a^0 40a^0$ (0.996)	3.142	19.87
	S_1	^1A	$38a^2 34b^2 35b^1 36b^1 39a^0 40a^0$ (0.991)	3.300	19.64
	S_2	^1A	$38a^2 34b^1 35b^2 36b^1 39a^0 40a^0$ (0.990)	4.144	19.84
$[Tcne\cdots Nap]_p$ (C_{2v})	S_0	$^1A_1$	$13a_2^2 21a_1^2 14a_2^1 17b_2^1 22a_1^0 16b_1^0$ (0.979)	0.0	~0
	T_1	$^1B_1$	$13a_2^2 21a_1^2 14a_2^1 17b_2^1 22a_1^0 16b_1^0$ (0.998)	3.563	19.64
	S_1	$^1B_1$	$13a_2^2 21a_1^2 14a_2^1 17b_2^1 22a_1^0 16b_1^0$ (0.997)	3.528	19.65
	S_2	$^1B_2$	$13a_2^2 21a_1^1 14a_2^2 17b_2^1 22a_1^0 16b_1^0$ (0.995)	4.131	19.63

[a] Only the molecular orbitals included in the active space are given. The expansion coefficient is given in *parentheses*

[b] Dipole moment at the direction from the center of Tcne to that of the donor

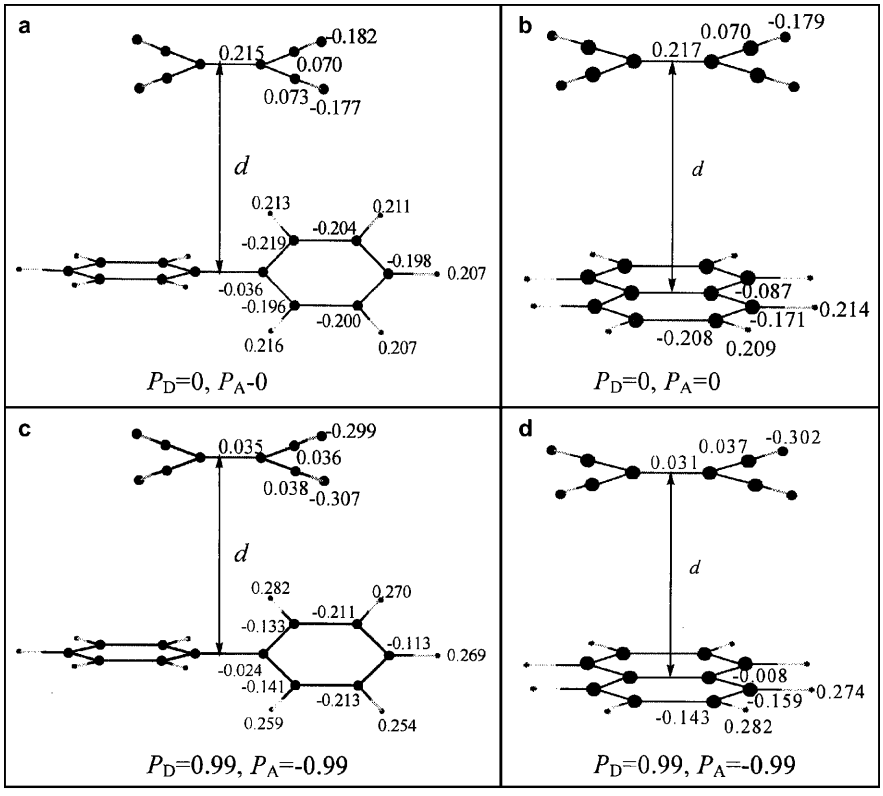

Fig. 3. Net charges on atoms for the ground states of **a** $[Tcne\cdots Bip]_p$ and **b** $[Tcne\cdots Nap]_p$, as well as for the first excited singlet states **c** $[Tcne^-\cdots Bip^+]_p$ and **d** $[Tcne^-\cdots Nap^+]_p$ after CASSCF (6, 6) calculations. d is the distance between the two centers of the donor and the acceptor. P_D is the net charge on the donor moiety, and P_A is that of the Tcne moiety. The applied symmetry is C_2 for $[Tcne\cdots Bip]_p$ and $[Tcne^-\cdots Bip^+]_p$, and C_{2v} for $[Tcne\cdots Nap]_p$ and $[Tcne^-\cdots Nap^+]_p$

Similar to the case of the ground state, Mulliken population analyses were applied for the purpose of investigating the charge distributions of the excited states. The net charges on atoms for S_1 states of $[Tcne\cdots Bip]_p$ and $[Tcne\cdots Nap]_p$ are given in Fig. 3c and d. Compared with the charge distribution of the ground state as shown in Fig. 3a and b, the changes of charge distribution can be considerable. Let us consider the charge distribution of the S_1 state of $[Tcne\cdots Bip]_p$. It can be found that the two central carbon atoms in Bip are almost neutral, whereas the positive charge spreads mainly on the other ten carbon atoms in Bip are almost neutral, whereas the positive charge spreads mainly on the other ten carbon atoms and the hydrogen atoms. On the other hand, the negative charge distributes mainly on the four nitrogen atoms and the two central carbon atoms of Tcne. Similarly, for the CT excited state S_1 of $[Tcne\cdots Nap]_p$, the state optimization shows that the two bridge-carbon atoms are neutral, with the positive charge distributing on the other carbon atoms and hydrogen atoms in Nap. By summing the net charges over the atoms in the donor moiety and Tcne acceptor moiety, we found that the net charge is +0.99 on the donor moiety but −0.99 on the Tcne moiety. Therefore the charge separation in S_1 states can be thought complete: this implies that the photoexcitation may directly lead to the ET from the donor moiety to the Tcne moiety. Apparently, a full charge separation must yield a large dipole moment (Table 2). Experimental results indicate that the photoexcitation of the EDA complex may directly lead to a singlet CT excited state [1, 18, 25]. From the Mulliken population analyses of moieties in the complex, we can find that S_1 states of the EDA complexes are CT excited states. Analogous conclusion

can be drawn for the S_2 states, namely, the ^1A state of $[Tcne\cdots Bip]_p$ and the $^1B_2$ state of $[Tcne\cdots Nap]_p$. It seems that the CT states optimized by us are just these from experimental observation, but accurate specifications of these states need further investigation, for example, the calculation of oscillator strengths and transition probabilities. These are not included in the present work. According to the Franck–Condon principle, the vertical transition energy, which is just the relative energy when taking the ground-state energy as zero, can be obtained from the calculation of the state energies (Table 2).

From the calculation of the CT excited states of C_2 symmetry for the $[Tcne\cdots Bip]_p$, we found that one of the two singly occupied molecule orbitals (SOMOs) in the S_1 state is a π-type orbital located on the Bip moiety and that the other is a π^*-type orbital contributed from the Tcne moiety. The largest component of the S_1 state is contributed mainly from the electron configuration of (core) $38a^2 34b^2 35b^1 36b^1 39a^0 40a^0$ (virt). Here we use (core) and (virt) to represent those MOs which remain doubly occupied and empty in the configuration interaction expansion, respectively. Compared with the ground state contributed mainly from the electron configuration (core) $38a^2 34b^2 35b^2 36b^0 39a^0 40a^0$ (virt), it can be found that the excitation from S_0 to S_1 results from an electron being promoted from the π-type highest occupied MO (HOMO) into the π^*-type lowest unoccupied MO (LUMO). The dipole moment of S_1 of $[Tcne\cdots Bip]_p$ is calculated to be 19.64 D in the direction from Tcne to Bip. Similarly, we found that S_2 of $[Tcne\cdots Bip]_p$ relates to the excitation of an electron out of the next HOMO into the LUMO; this configuration can be represented as (core) $38a^2 34b^1 35b^2 36b^1 39a^0 40a^0$ (virt). The S_2 state of $[Tcne\cdots Bip]_p$ is also a CT state, and the large dipole moment, 19.84 D in the direction from Tcne to Bip, of this state can be thought to be substantially the same as that of the S_1 state. The energy gap between the S_1 state and the S_2 state is found to be 0.844 eV.

For $[Tcne\cdots Nap]_p$ of C_{2v} symmetry, the lowest CT excited state has its largest component contributed from the electron configuration of (core) $13a_2^2 21a_1^2 14a_2^1 17b_2^1 22a_1^0 16b_1^0$ (virt). From the expansion coefficients of the electron configurations after CASSCF calculation of the CT excited state, it was found that the S_1 state of $[Tcne\cdots Nap]_p$ arises from an electron being promoted from the π-type HOMO into the π^*-type LUMO of the complex. The dipole moment of the S_1 state of $[Tcne\cdots Nap]_p$ is calculated to be 19.65 D in the direction from Tcne to Nap. In S_2 of $[Tcne\cdots Nap]_p$, one electron is prompted from the next HOMO into the LUMO; the main configuration can be represented as (core) $13a_2^2 21a_1^1 14a_2^2 17b_2^1 22a_1^0 16b_1^0$ (virt). The S_2 state of $[Tcne\cdots Nap]_p$ is also a CT state, and possesses a large dipole moment of 19.63 D. The energy gap between the S_1 state and the S_2 state of $[Tcne\cdots Nap]_p$ is found to be 0.603 eV.

From the CASSCF calculations, we also found that the lowest triplet excited state, T_1, is a CT excited state as well; however, unlike the usual T_1 state, the CT state T_1 possesses almost the equivalent state energy as the S_1 state at the geometry of the EDA complex. This is true for both $[Tcne\cdots Bip]_p$ and $[Tcne\cdots Nap]_p$. In the case of $[Tcne\cdots Nap]_p$, the S_1 state even lies below the T_1 state. In fact, the complex in the CT excited state is more likely to be a diradical. It seems that being singlet or being triplet does not dominate the state energy in such cases.

3.3 Excited state at equilibrium geometry of the ion pair

The ion pairs characterized by CT emissions have been proved to be the key to accurately determining the parameters controlling back ET reactions [25]. The ion pair may dissociate to free ions or undergo CR to reform the ground-state EDA complex. In the CR, the neutral acceptor and donor are regenerated. In obtaining the equilibrium geometry of the ion pair, we firstly only optimized the center-to-center distance, d, between the donor cation and the acceptor anion through the potential-energy surface construction, keeping the geometries of isolated optimized donor cation and the acceptor anion fixed. It should be pointed out that the structure of the Bip^+ ion is planar rather than torsional. The C_{2v} symmetry constraint was been employed in searching for the maximum of the stabilization energy, and the counterpoise method of Boys and Bernadi was also applied for the BSSE correction [22, 23, 24]. We used the unrestricted HFSCF method to perform the calculation of the triplet, so as to find an equilibrium center-to-center distance of the ion pair. The center-to-center distance was determined on the basis of the counterpoise-corrected potential-energy surface. The counterpoise-corrected stabilization energy (E_s^{cp}) of the ion pair is defined in the same way as that of the EDA complex, and it reaches a maximum value of 229.408 kJ mol^{-1} for $[Tcne\cdots Bip]_s$ at $d = 0.37$ nm, and 239.215 kJ mol^{-1} for $[Tcne\cdots Nap]_s$ at $d = 0.36$ nm. In the case of no BSSE correction, we found that E_s reaches the maximum at $d = 0.36$ nm for $[Tcne\cdots Bip]_s$ and $d = 0.35$ nm for $[Tcne\cdots Nap]_s$. Differing from the EDA complex, the ion pair possesses an extremely large stabilization energy; this is resulted from the Coulomb interaction. Maintaining the equilibrium center-to-center distance fixed, full geometry optimizations of ion pairs of the triplet were also performed at the level of UHF/6-31G, but only slight changes of bond parameters were found. A notable appearance in the fully optimized geometries is that all the carbon atoms in the donor moiety remain planar, but the hydrogen atoms slightly approach the Tcne moiety.

On the basis of the geometries obtained from UHF/6-31G optimizations, the S_1 and T_1 states of the ion pairs were calculated at the level of CASSCF (6,6)/6-31G with C_{2v} symmetry. Just as in the case of the EDA complex, three π-type MOs and three π^*-type MOs were included in the configuration interaction expansion. The results are listed in Table 3. Similar to the S_1 state in the EDA complex, the highest SOMO in the S_1 state is found to be a π^*-type MO located on Tcne. The next highest SOMO is also found to be a π-type MO contributed mainly from the carbon atoms in the donor, say, Bip or Nap. Both

Table 3. State energies of the ion pair using a CASSCF/6-31G calculation in the gas phase. The relative energy with the relative energy of the S_0 state in ion pair geometry being zero. The energies of the ground states of $[Tcne\cdots Bip]_s$ and $[Tcne\cdots Nap]_s$ are −904.78109 and −827.92132 au, respectively

	State[a]	Symmetry	Main configuration[b]	RE/eV	D/D[c]
$[Tcne\cdots Bip]_s$	S_0	$^1A_1$	$23a_1^2 15a_2^2 20b_2^2 21b_2^0 24a_1^0 22b_2^0$ (1.000)	0.0	~0
(C_{2v}, d = 0.37 nm)	T_1	$^3A_1$	$23a_1^2 15a_2^2 20b_2^2 21b_2^1 24a_1^0 22b_2^0$ (0.999)	1.870	15.80
	S_1	$^1A_1$	$23a_1^2 15a_2^2 20b_2^2 21b_2^1 24a_1^0 22b_2^0$ (0.962)	1.944	15.24
$[Tcne\cdots Nap]_s$	S_0	$^1A_1$	$13a_2^2 21a_1^2 14a_2^2 17b_2^0 16b_1^0 22a_1^0$ (0.996)	0.0	~0
(C_{2v}, d = 0.36 nm)	T_1	$^3B_1$	$13a_2^2 21a_1^2 14a_2^1 17b_2^1 16b_1^0 22a_1^0$ (0.999)	1.841	14.92
	S_1	$^1B_1$	$13a_2^2 21a_1^2 14a_2^1 17b_2^1 16b_1^0 22a_1^0$ (0.999)	1.796	14.96

[a] S_0 is the charge recombination state at the ion pair geometry
[b] The expansion coefficient is given in *parentheses*
[c] Dipole moment in the direction from the center of Tcne to that of the donor

the S_1 state and the T_1 state of $[Tcne^- \cdots Bip^+]_s$ have A_1 symmetry, and the largest components of both are contributed mainly from the electron occupation (core) $23a_1^2 15a_2^2 20b_2^1 21b_2^1 24a_1^0 22b_2^0$ (virt). The T_1 state of $[Tcne^- \cdots Bip^+]_s$ lies below the S_1 state by 0.074 eV. For $[Tcne^- \cdots Nap^+]_s$, both the S_1 and T_1 states of the ion pair have a B_1 symmetry, and their largest components are contributed mainly from a configuration of (core) $13a_2^2 21a_1^2 14a_2^1 17b_2^1 16b_1^0 22a_0^1$ (virt). We found that the S_1 state of $[Tcne^- \cdots Nap^+]_s$ lies below the T_1 state by 0.045 eV. The sequence of the states in the ion pair is the same as that of the EDA geometry.

Partial bonding between donors and acceptors was originally proposed by Mulliken [26], and ab initio calculation confirmed the incipient bonding in the related ethylene cation–radical complex [27]. We examined the overlap population analyses of ion pairs in our calculations but bonding, even incipient bonding between donors and acceptor in the systems we studied, was not been found, possibly owing to the large intervening donor–acceptor distance.

4 Solvent effects on CT absorption

In order to make the theoretical calculation be comparable with experimental observation, the solvent reorganization energy on the CT absorption spectra needs to be considered [28, 29, 30, 31, 32, 33]. Since the fast vertical transition does not permit the solvent molecules to adjust their orientation polarization according to the new charge distribution of the solute, the so-called solvent reorganization energy frequently appears in the literature on ET and spectra discussions. In the investigation of the solvent effects on CT absorption, the solvation energies contributed from the fast (electronic) response and the slow (orientational) response should be taken into account separately. On the basis of the gas-phase calculation of the state energies, we consider the solvent effects on the ground state and the excited states using the Onsager model [34], although such treatment at present can only give semiquantitative results. In this approach, the solute is regarded to be encompassed in a spherical cavity of radius a_0, the solvent are taken as a dielectric continuum, and the solvation energy is estimated by considering the interaction between the point dipole of the solute and the reaction field resulting from the solvent polarization. The equilibrium solvation energy of state i is given by [34]

$$E_i^{\text{solv}} = -1/2\mu_i R \tag{6}$$

where μ_i is dipole moment of ith state and R the solvent reaction field. The reaction field depends on the magnitude and direction of the dipole moment and gives rise to the solvent polarization. In absorption, the initial (ground) state is fully equilibrated with the solvents, and the reaction field can be given by

$$R = \frac{2}{a_0^3}\mu_g\left\{\frac{\varepsilon - 1}{2\varepsilon + 1}\right\} \ , \tag{7}$$

where ε is the static dielectric constant of the solvent.

The solvation energy of ground state is thus

$$E_g^{\text{solv}} = -\frac{1}{a_0^3}\mu_g \cdot \mu_g\left\{\frac{\varepsilon - 1}{2\varepsilon + 1}\right\} \ , \tag{8}$$

where μ_g is the dipole moment of the ground state, a_0 is the radius of the cavity, and ε is the static dielectric constant of the solvent. According to the Franck–Condon principle, during the vertical transition from the ground state to the excited state, only the electronic response of the solvents can catch up with the change of the solute charge distributions; thus, the reaction field felt by the final state arising from the orientational part of the solvent polarization is just that felt by the fully relaxed ground state. Therefore, similar to Eq. (7), the static reaction field felt by the final state can be expressed as

$$R' = \frac{2}{a_0^3}\mu_g\left\{\frac{\varepsilon - 1}{2\varepsilon + 1} - \frac{n^2 - 1}{2n^2 + 1}\right\} \ , \tag{9}$$

where n^2 is the optical dielectric constant. Since the interaction energy between the excited state dipole, μ_e, and the static field should be $-\mu \cdot R'$, without further consideration of the solvent polarization cost, the solvation energy can be expressed as

$$E_e^{\text{solv}} = -\frac{1}{a_0^3}\left[2\mu_e \cdot \mu_g\left\{\frac{\varepsilon - 1}{2\varepsilon + 1} - \frac{n^2 - 1}{2n^2 + 1}\right\} + \mu_e \cdot \mu_e\left\{\frac{n^2 - 1}{2n^2 + 1}\right\}\right] \ , \tag{10}$$

where μ_e is the dipole moment of the excited state, and we use e to refer to the excited (final) state. The second term in the bracket is the interaction between μ_e and the field produced by the electronic polarization of the excited state. In the calculation, we replace the dipole moment in dichloromethane with the gas-phase value.

The vertical transition energy from the ground state to the excited state in solution is thus

$$E_{g\to e}^{sol} = E_{g\to e}^{gas} + E_e^{solv} - E_g^{solv} \quad , \tag{11}$$

The choice of the cavity radius, a_0, has been the subject of many discussions. In this work, we employed the Hyperchem package to calculate the equivalent cavity volume, V_M, of the complex. The EDA complex is close to a spherical shape; thus, we adopted the following procedure to estimate the spherical cavity radius, a_0 [35]:

1. Replace water molecules with the EDA complex in a water periodic box in Hyperchem, with the minimum distance between the solvent and solute atoms being 0.23 nm.
2. Use the number, n, actually an average value, of the substituted water molecules to obtain the solute molecular volume, V_M,$V_M = nV_m$, with $V_m = 0.02992$ nm^3 being the molecular volume of H_2O.
3. Use Eq. (12) to determine the equivalent cavity radius, a_0, of the solute:

$$a_0 = (3V_M/4\pi)^{1/3} \quad . \tag{12}$$

Substitute the estimated cavity radii for a_0 in Eqs. (8) and (10). According to Eq. (12), the a_0 is 0.368 nm for $[Tcne\cdots Bip]_p$, and 0.400 nm for $[Tcne\cdots Nap]_p$. Our results for the solvent effect on the vertical absorption transition energies are given in Table 4. For the convenience of comparison, dichloromethane ($\varepsilon = 9.08$ [36], $n = 1.425$ [37]) was chosen as the solvent.

Compared with values of the transition energy in the gas-phase (Table 2), we can find that a redshift of the CT absorptions appears in dichloromethane. The wavelength of the maximum absorbance band corresponding to the $S_0 \rightarrow S_1$ transition of $[Tcne\cdots Bip]_p$ in the gas phase is 375.7 nm, while it is 498.9 nm in dichloromethane. Owing to the existence of larger dipole moments of about 20 D the solvation energies are -0.817 eV for the S_1 state and -0.833 eV for the S_2 state; these are much larger than that of the ground state. Another value of the wavelength, 374.2 nm, which corresponds to the transition from the S_0 state to the S_2 state, is obtained. In the experimental aspect, Hubig et al. [1] measured the CT absorptions by using time-resolved (femtosecond) spectroscopy. The wavelengths of the CT absorptions were obtained to be 500 and 400 nm in dichloromethane [1].

For $[Tcne\cdots Nap]_p$, the charge separation of both the S_1 and the S_2 states produces a solvation energy of about -0.75 eV in dichloromethane, owing to the large dipole moments. Unlike the case of $[Tcne\cdots Bip]_p$, if we have a look at the results listed in Table 4, we can find large discrepancies between our calculations and the experimental measurements. After taking the solvent effect of the transition energies into consideration, we have given a prediction of the absorption wavelength of 443.3 nm for the $S_0 \rightarrow S_1$ transition and 364.6 nm for the $S_0 \rightarrow S_2$ transition; such predocations greatly differ from the experimental measurements of 550 nm and 426 nm by Merrifield and Phillips in 1958 [18]. The interpretation of what causes such large discrepancies should be addressed. We cannot, at present at least, give a convincing explanation for this. We have only found the experimental data on the CT absorption of this system by Merrifield and Phillips. For unknown reasons, although a lot of experiments on different Tcne-donor systems have been repeated since then, we have failed to find other experimental values for this system. In addition, from another view, a sequence of the wavelengths of the maximum absorbance can be determined by Eq.(3). Both our theoretical calculation and the experimental measurement show that Nap possesses a larger IP value than Bip does (Table 2); hence, a shorter wavelength for $[Tcne\cdots Nap]_p$ than for $[Tcne\cdots Bip]_p$ can be predicted. In fact, from Eq. (3), a value of 454 nm for the $S_0 \rightarrow S_1$ transition, which coincides with our theoretical result, can be predicted. Even though, since the results of the solvent effect obtained in the framework of the Onsager model is very qualitative, we are not sure whether the discrepancy of the wavelengths of the CT absorptions between our calculation and experiment is caused by the inaccuracy of our theoretical calculations. Further investigation on this system is needed. It should be mentioned that the good agreement of the transition energy of $[Tcne\cdots Bip]_p$ between theoretical calculation and experimental measurement does not mean that we have achieved the accurate description of the realistic CT absorption, since the realistic environment is much more complicated than what we can theoretically simulate; however, these results can, at least, confirm the appropriateness of our theoretical treatments.

5 Discussions and conclusions

All ab initio calculations were carried out using HONDO 99 [38]. For $[Tcne\cdots Bip]_p$ and $[Tcne\cdots Nap]_p$, it was found that the S_1 and the S_2 states of the EDA complex

Table 4. Solvation energies and vertical transition energies of the transitions $S_0 \rightarrow S_1$ and $S_0 \rightarrow S_2$ in dichloromethane. According to Eq. (12), the radius, a_0, is calculated to be 0.368 nm for $[Tcne\cdots Bip]_p$, and 0.400 nm for $[Tcne\cdots Nap]_p$

	Transition	$E_{g\to e}^{gas}$/eV	E_g^{solv}/eV[a]	E_e^{solv}/eV	λ_{CT}/nm	λ_{CT}/nm (expt.)[b]
$[Tcne\cdots Bip]_p$	$S_0 \rightarrow S_1$	3.300	−0.002	−0.847	505.0	500
(C_2)	$S_0 \rightarrow S_2$	4.144	−0.002	−0.863	377.7	400
$[Tcne\cdots Nap]_p$	$S_0 \rightarrow S_1$	3.528	−0.001	−0.748	445.9	550[c]
(C_{2v})	$S_0 \rightarrow S_2$	4.131	−0.001	−0.747	366.3	426[c]

[a] Since the dipole moments of the ground states are negligibly small as shown in Table 2, the values of the solvation are quite small

[b] The values of the charge-transfer absorptions observed in experiments

[c] The wavelength of the maximum absorbance band corresponding to the $S_0 \rightarrow S_1$ transition of $[Tcne\cdots Nap]_p$ in dichloromethane is estimated to be 454 nm from Eq. (3)

are CT excited states, and the photoexcitation corresponding to the $S_0 \rightarrow S_1$ and $S_0 \rightarrow S_2$ transitions of the EDA complex may result in a new absorption in the visible region. This new absorption apparently differs from those of the isolated donor and acceptor. From charge distribution and MO occupation situation, we have ascertained that the CT absorption arises from the electron transition from the π-type HOMO, which locates on the arene moiety, to the π^*-type LUMO which locates on the Tcne moiety. Our calculations provide evidence to supplement the experimental observations. Considering the relaxation of the CT excited state to its equilibrium geometry, the successive complexes that correspond to the CT excited state have been determined.

The dipole moments used for the solvent reorganization energy correction should be those obtained in the solvent environment, rather than in the gasphase, since, in general, polar solvents can influence the dipole moment of the solute; however, in our cases, the parallel arrangement of the donor and the acceptor in the complex confines the distribution of the electron density and thus the dipole moment in solution can be predicted not to change too much from the gas-phase case. This encourages us to use the gas-phase dipole moment in the solvent reorganization energy correction. Comparing the calculated CT absorption in the gas phase with the calculated value in the polar solvent of dichloromethane reveals a redshift for both $[\text{Tcne}\cdots\text{Bip}]_p$ and $[\text{Tcne}\cdots\text{Nap}]_p$. From Eq. (11), one can see that since the initial state possesses a dipole moment close to zero, the net effect produced by polar solvents upon the absorption spectra is the decrease of the transition energy.

Acknowledgements. This work was supported by the Natural Science Foundation of China (29892164, 39970183) and the State Key Laboratory of Theoretical and Computational Chemistry in Jilin University.

References

1. Hubig SM, Bockman TB, Kochi JK (1996) J Am Chem Soc 118: 3842
2. Tung CH, Zhang LP, Li Y, Cao H, Tanimoto Y (1997) J Am Chem Soc 119: 5348
3. Frey JE, Andrews AM, Ankoviac DG, Ankoviac DG, Beaman DN, Pont LED, Elsner TE, Lang SR, Zwart MAO, Seagle RF, Torreano LA (1990) J Org Chem 55: 606
4. Haga N, Nakajima H, Takayanagi H, Tokumaru K (1998) J Org Chem 63: 5372
5. Grasselli JG, Ritchey WM (1975) Atlas of spectral data and physical constants for organic compounds III. CRC, Ohio, p 282
6. Dixon DA, Miller JS (1986) J Am Chem Soc 109: 3656
7. Grasselli JG, Ritchey WM (1975) Atlas of spectral data and physical constants for organic compounds II. CRC, Ohio, p 537
8. Tsuzuki K, Tanabe K (1991) J Phys Chem 95: 139
9. (a) Li XY, Xiao SQ, He FC (1999) J Comput Chem 20: 597 (b) Li XY, Tong J, He FC (2000) Chem Phys 260: 283
10. Bredas JL, Street GB, Themans B, André JM (1985) J Chem Phys 83: 1323
11. Rubio M, Merchan M, Orti E (1995) Chim Acta 91: 17
12. Tsuzuki S, Tanabe K (1991) J Phys Chem 95: 139
13. El-Kemary MA (1995) J Photochem Photobiol A Chem 87: 203
14. Dean JA (ed) (1999) Lange's handbook of chemistry, 15th edn. McGraw-Hill, New York, pp 4.8, 4.16
15. Bricgleb G (1964) Angew Chem 8: 326
16. Bricgleb G, Czekalla Z (1959) Elektrochem 63: 6
17. Li XY, Zhou C, Li ZR, Qiu L (2000) Acta Chim Sin 58: 189
18. Merrifield RE, Phillips WD (1958) J Am Chem Soc 80: 2778
19. Becker H-C, Broo A, Nordén B (1997) J Phys Chem A 101: 8853
20. Casrella M, Millié P, Piuzzi F, Caillet J, Langlet J, Claverie P, Tramer A (1989) J Phys Chem 93: 3941
21. Boys SF, Bernardi F (1970) Mol Phys 19: 553
22. Van Duijneveldt FB, de Rijdt Van Duijneveldt JGCM, van Lenthe JH (1994) Chem Rev 94: 1873
23. Alagona G, Ghio C, Tomasi J (1989) J Phys Chem 93: 5401
24. Sim F, St-Amant A, Papai I, Salahub DR (1992) J Am Chem Soc 114: 4391
25. (a) Gould IR, Farid S (1996) Acc Chem Res 29: 522; (b) Gould IR, Farid S, Young R (1992) J Photochem Photobiol A Chem 65: 133
26. (a) Mulliken RS (1952) J Am Chem Soc 811; (b) Mulliken RS (1952) J Phys Chem 801
27. Alvrez-Idaboy JR, Eriksson LA, Fängström T, Lunell S (1996) J Phys Chem 97: 12737
28. Cramer CJ, Truhlar DG (1999) Chem Rev 99: 2161
29. Jean JM, Hall KB (2000) J Phys Chem A 104: 1930
30. Naka K, Morita A, Kato S (1999) J Chem Phys 110: 3484
31. Klamt A, Jonas V, Bürger T, Lohrenz JCW (1998) J Phys Chem A 102: 5074
32. Herbich J, Kapturkiewicz A (1998) J Am Chem Soc 120: 1014
33. Gould IR, Young RH, Mueller LJ, Farid S (1994) J Am Chem Soc 116: 8176
34. Onsager L (1936) J Am Chem Soc 58: 1486
35. Li XY, Zhao LL, Xiao SQ (2000) Theor Chem Acc 105: 77
36. Weast RC, Astle MJ (1982–1983) CRC Handbook of Chemistry and Physics, 63rd edn. CRC, Boca Raton, p E-51
37. Dean JA (ed) (1999) Lange's handbook of chemistry, 15th edn. McGraw-Hill, New York, p 11.17
38. Dupuis M, Marquez A, Davidson ER (1999) "HONDO 99" based on HONDO95.3 by Dupuis M, Marquez A, Davidson ER, Quantum Chemistry Program Exchange, Indiana University, Blomington, IN 47405, USA